Applied Catalysis B: Environmental 219 (2017) 450–458

Contents lists available at ScienceDirect

Applied Catalysis B: Environmental

journal homepage: www.elsevier.com/locate/apcatb

ResearchPaper

Exploring the photocatalysis mechanism on insulators

Fan Dong[a,*], Ting Xiong[a], Yanjuan Sun[a], Lilin Lu[b,*], Yuxin Zhang[c], Haijun Zhang[b], Hongwei Huang[d], Ying Zhou[e], Zhongbiao Wu[f,*]

[a] Chongqing Key Laboratory of Catalysis and New Environmental Materials, College of Environment and Resources, Chongqing Technology and Business University, 400067, Chongqing, China
[b] College of Chemical Engineering and Technology, The State Key Laboratory of Refractories and Metallurgy, Wuhan University of Science and Technology, Wuhan, 430081, China
[c] College of Materials Science and Engineering, National Key Laboratory of Fundamental Science of Micro/Nano-Devices and System Technology, Chongqing University, Chongqing, 400044, China
[d] School of Materials Science and Technology, National Laboratory of Mineral Materials, China University of Geosciences, Beijing, 100083, China
[e] The Center of New Energy Materials and Technology, School of Materials Science and Engineering, Southwest Petroleum University, Xindu Rd. 8, Chengdu, 610500, China
[f] Department of Environmental Engineering, Key Laboratory of Environment Remediation and Ecological Health of Ministry of Education, Zhejiang University, Hangzhou, 310058, China

ARTICLE INFO

Article history:
Received 2 June 2017
Received in revised form 20 July 2017
Accepted 26 July 2017
Available online 29 July 2017

Keywords:
Photocatalysis mechanism
Insulator
Oxygen defects
Environmental remediation

ABSTRACT

Photocatalysis is a promising technology for addressing environmental and energy issues. Most photocatalysts are semiconductors, while a minority are metals. Unlike these two types of materials, insulators display a large band gap separating occupied and unoccupied levels. However, it is still possible to excite charge carriers in insulators via specific defects. Herein, we report an insulating carbonate ($BaCO_3$) that displayed photocatalytic activity towards the removal of NO in air. The oxygen defects produced during the preparation process endow the as-prepared carbonate with the ability to generate charge carriers for oxidation of NO under UV light irradiation. Furthermore, other salts, such as sulphate and phosphate insulators, have also been observed to possess photocatalytic activity. These findings suggest that this new family of earth-abundant insulator photocatalysts can provide promising opportunities for photo-energy conversion and environmental remediation, opening up a new direction in catalysis science.

1. Introduction

Over the past few decades, increasing attention has been drawn toward photocatalytic materials for environmental remediation and green energy production [1–6]. On the one hand, owing to their suitable band gap, semiconductors, such as typical TiO_2 and graphitic carbon nitride (g-C_3N_4), have been extensively studied as photocatalysts and applied in many important areas [7–11].On the other hand, conductors, such as plasmonic metals, can also function as photocatalysts to yield charge carriers and photo-catalyse some chemical reactions because of surface plasmon resonance [12,13].

However, little attention has been paid to insulators in photocatalysts development because of their relatively large band gap, which prevents electron excitation from the valence band (VB) to the conduction band (CB) under light irradiation. Despite many attempts to explore the properties of insulators, to the best of our knowledge, there have been few successful cases of the use of these materials for photocatalytic reactions [14].

Herein, we report for the first time the unexpected and promising photocatalytic activity of $BaCO_3$, a typical insulator that is commonly used in the ceramics industry as a glaze ingredient [15,16], in removal of nitrogen oxide (NO) from air. The underlying photocatalysis mechanism is discussed and elucidated based on experimental studies and first-principles calculations. Our results demonstrate that the O-vacancy defects present in the $BaCO_3$ sample play dominant roles in the photocatalytic removal of NO. Interestingly, other insulating salts, including carbonates ($SrCO_3$), sulphates ($SrSO_4$, $BaSO_4$) and phosphates ($Sr_3(PO_4)_2$), have also been found to show photocatalytic performance. To our knowledge, this is an unprecedented report on the photocatalysis of widely available insulating materials and can open up a new direction in catalysis science.

* Corresponding authors.
E-mail addresses: dfctbu@126.com (F. Dong), lulilin@wust.edu.cn (L. Lu), zbwu@zju.edu.cn (Z. Wu).

http://dx.doi.org/10.1016/j.apcatb.2017.07.082
0926-3373/

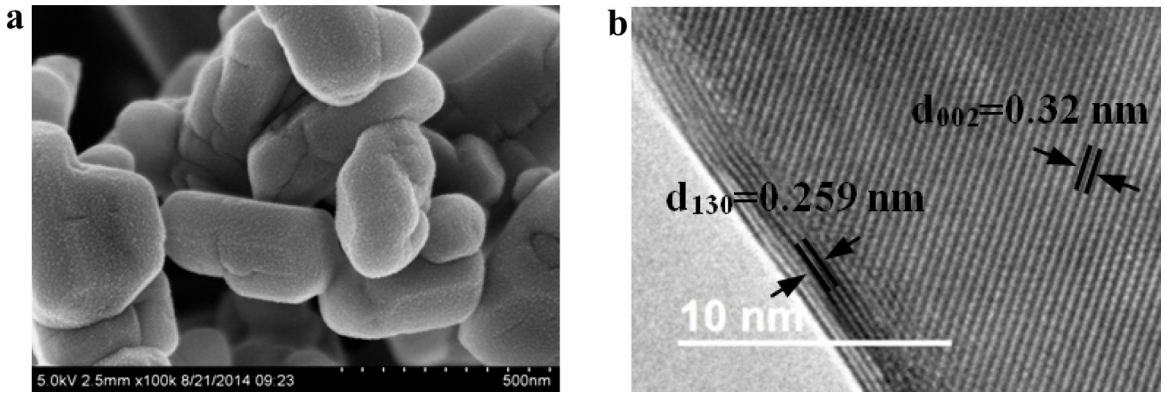

Fig. 1. (a) SEM image. (b) HRTEM image.

2. Experimental section

2.1. Preparation of photocatalysts

$BaCO_3$ were prepared from Na_2CO_3 and $Ba(NO_3)_2$ at room temperature. Typically, 2.12 g of Na_2CO_3 (20 mmol) was dissolved in 70 mL of water, followed by dropwise addition of $Ba(NO_3)_2$ (5.22 g, 20 mmol) dissolved in 60 mL of water into the above aqueous solution. The mixture was stirred for 1 h and then precipitated for another 1 h. The precipitate was separated by centrifugation and washed with deionized water and absolute ethanol several times. Finally, the as-obtained product was dried at 60 °C for further characterization. $BaSO_4$, $SrSO_4$, $SrCO_3$ and $Sr_3(PO_4)_2$ were all synthesized at room temperature under reaction conditions similar to those for $BaCO_3$.

$BaSO_4$ samples were prepared from Na_2SO_4 (20 mmol) and $Ba(NO_3)_2$ (20 mmol).

$SrSO_4$ samples were prepared from Na_2SO_4 (20 mmol) and $Sr(NO_3)_2$ (20 mmol).

$SrCO_3$ samples were prepared from Na_2CO_3(20 mmol) and $Sr(NO_3)_2$ (20 mmol).

$Sr_3(PO_4)_2$ samples were prepared from Na_3PO_4 (20 mmol) and $Sr(NO_3)_2$ (30 mmol).

2.2. Photocatalytic activity measurements

The as-prepared samples were all used for photocatalytic removal of NO at the ppb level in a continuous flow reactor under UV light irradiation. The reactor was 4.5 L (30 cm × 15 cm × 10 cm), made of polymeric glass, and covered with Saint-Glass. A UV lamp (8 W) was used as the light source (280 nm). The as-prepared sample (0.20 g) was dispersed in distilled water (50 mL) in a beaker via ultrasonic treatment for 10 min and then coated onto two glass dishes (12.0 cm in diameter). The coated dishes were pretreated at 70 °C to remove the water in the suspension and were placed at the centre of the reactor. The NO gas was acquired from a compressed gas cylinder at a NO concentration of 100 ppm (N_2 balance). The initial concentration of NO was diluted to 600 ppb. The flow rates of the air stream and NO were controlled at 2.4 L/min and 15 mL/min, respectively. The two gas streams were then premixed in a three-way valve. The relative humidity was controlled at 50% in the air stream. Upon achieving the adsorption-desorption equilibrium, the lamp was turned on. The concentration of NO was measured every min by using a NOx analyser (Thermo Scientific, 42i-TL) that also monitored the concentrations of NO_2 and NOx (NOx represents NO + NO_2). The NO removal ratio (η) was calculated using η (%) = $(1 - C/C_0) \times 100\%$, where C is the outlet concentration of NO after the reaction for time t and C_0 represents the inlet concentration after achieving adsorption-desorption equilibrium.

Photocatalytic activity of the samples for degradation of aqueous methyl orange (MO) was evaluated in a glass reactor; 0.20 g of the as-prepared samples was dispersed in an MO aqueous solution (100 mL, 8.0 mg/L). The suspension was allowed to reach equilibrium with continuous stirring for 30 min in the dark. An 8 W UV lamp (λ = 280 nm) was used as the UV light source to trigger the photocatalytic reaction. During irradiation, 5 mL of suspension was continually taken from the reaction cell at given time intervals for subsequent dye concentration analysis after centrifuging. The degradation efficiency of MO was evaluated by using the UV–vis absorption spectra to measure the peak value of the maximum absorption of the MO solution at a wavelength of 464 nm.

2.3. In situ *DRIFTS study*

In situ DRIFTS experiments were carried out using FT-IR spectrometers (Bruker Tensor II) equipped with an in situ diffuse-reflectance cell (Harrick), which contained three windows, including two KBr windows for IR measurements and a quartz window for light irradiation using a KL 2500 LCD lamp (SCHOTT). The catalyst bed was 3 mm deep and contained a 2.4 mm layer of inert-sieved SiO_2 particles with a 0.6 mm photocatalyst layer on the top of the SiO_2. The photocatalyst was pretreated at room temperature under He (100 mL/min) for 60 min to remove adsorbed impurities. After the background spectrum was recorded with flowing He and then subtracted, the sample was then exposed to 50 ppm of NO (50 mL/min). When the adsorption-desorption equilibrium was achieved, the UV lamp (MUA-165) was turned on. The DRIFTS spectra of the samples were recorded at room temperature by accumulating 32 scans with a resolution of 4 cm^{-1} at a given interval. The illustration of the designed reaction system for the in situ DRIFTS apparatus and photo of the DRIFTS system under working are shown in Scheme S1 in the Supplementary Information.

2.4. Catalyst characterization

The crystal phases of the sample were analysed by X-ray diffraction (XRD) using Cu Kα radiation (model D/max RA, Rigaku Co., Japan). Scanning electron microscopy (SEM; model JSM-6490, JEOL, Japan) and transmission electron microscopy (TEM; JEM-2010, Japan) were used to characterize the morphology and structure of the obtained products. X-ray photoelectron spectroscopy (XPS) with Al Kα X-rays (hm = 1486.6 eV) radiation operated at 150 W (Thermo ESCALAB 250, USA) was used to investigate the surface properties. Nitrogen adsorption–desorption isotherms were

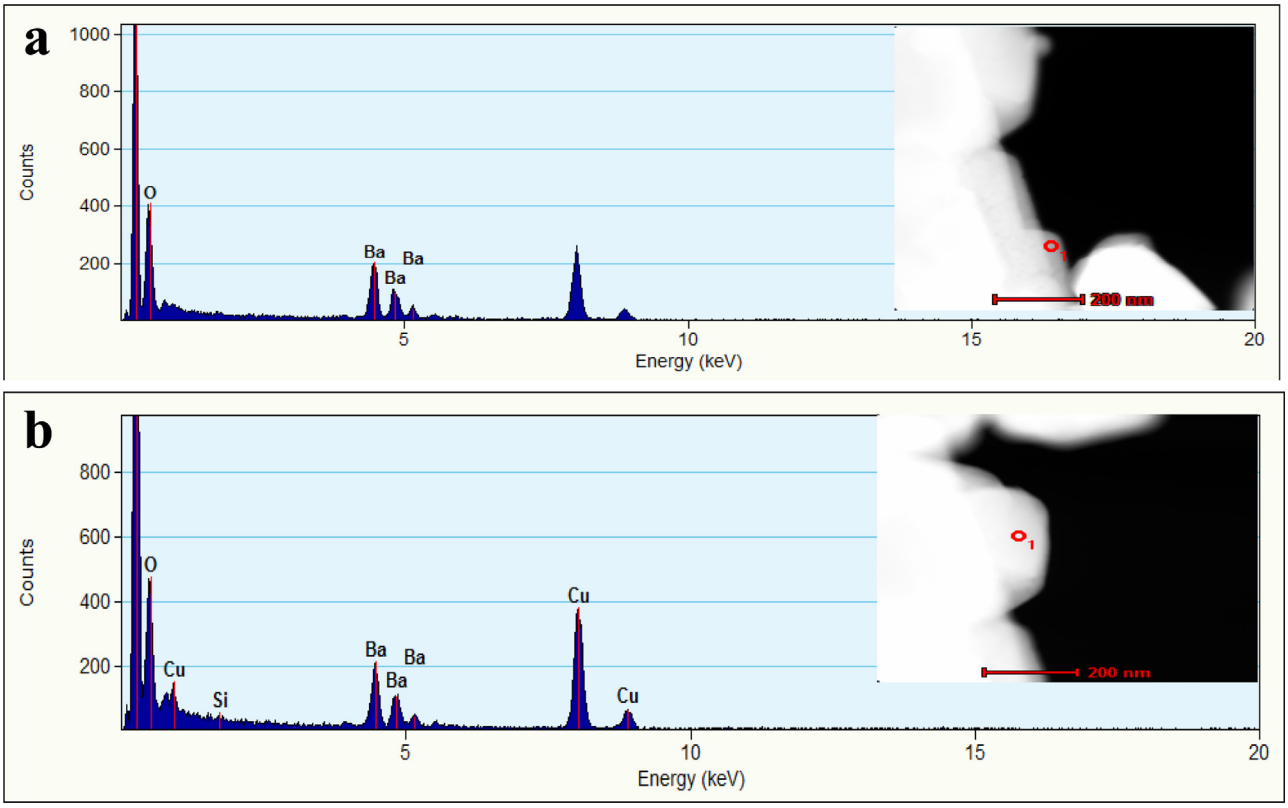

Fig. 2. (a) The EDX point scan of the surface of $BaCO_3$. (b) The EDX point scan of the bulk of $BaCO_3$.

obtained using a nitrogen adsorption apparatus (ASAP 2020, USA). The samples were degassed at 120 °C prior to measurements. UV–vis diffuse-reflectance spectrometry (DRS) spectra were obtained for the dry-pressed disk samples using a Scan UV–vis spectrophotometer (TU-1901, China) equipped with an integrating sphere assembly using 100% $BaSO_4$ as the reflectance sample. All of the photoelectrochemical measurements were conducted in a three electrode system on a CHI 660D electrochemical work station using FTO glass with $BaCO_3$ films as the working electrode, saturated calomel electrode as the reference electrode and Pt wire as the counter electrode. All of the potentials are quoted with respect to the saturated calomel electrode. The working electrode was irradiated from the $BaCO_3$ films (250 mg of as-prepared $BaCO_3$ nanoparticles were suspended in 0.5 mL of DMF, which was then dip-coated on a 10 mm × 10 mm FTO glass electrode. The electrode was then annealed at 170 °C for 2 h. The photocurrent time-dependence of $BaCO_3$ films at the open circuit potential was measured in 0.5 M Na_2SO_4 under chopped illumination with 40 s light on/off cycles per side under a UV lamp. The sample for the electron spin resonance (ESR) measurement was prepared by mixing $BaCO_3$ in a 50 mM DMPO solution tank (aqueous dispersion for DMPO-·OH and methanol dispersion for DMPO-$^{\bullet}O_2^-$). UV light at the wavelength of 280 nm was used to irradiate the sample. Additionally, electron paramagnetic resonance (EPR) spectra were collected using a Bruker ESP 500 spectrometer at 77 K in the dark and under light irradiation at a wavelength of 280 nm. Steady and time-resolved fluorescence emission spectra were recorded at room temperature using a fluorescence spectrophotometer (Edinburgh Instruments, FLSP-920). To determine the involvement of active species during photocatalysis over $BaCO_3$, we performed trapping experiments for the detection of holes (h^+) and electrons (e^-) in the photocatalytic process. The scavengers used in this research were potassium dichromate ($K_2Cr_2O_7$, 1%) for e^- and potassium iodide (KI, 1%) for h^+.

2.5. Computational methodology

First-principles calculations were performed using the Cambridge Serial Total Energy Package (CASTEP) code based on the density functional theory (DFT) [17]. The electron exchange and correlation energies were calculated within the generalized gradient approximation (GGA) using the Perdew-Burke-Ernzerhof (PBE) functional [18]. The interactions between the core region and valence electrons were described by ultrasoft pseudopotentials (USP). The equilibrium geometries of all of the investigated unit cells were determined by performing optimization without any symmetry constraint using the Broyden-Fletcher-Goldfarb-Shannon (BFGS) minimization method. The cell parameters and atomic coordinates were fully optimized. The self-consistent-field (SCF) convergence criterion was set to the root-mean-square (rms) change in the electronic density less than 2.0×10^{-6} eV/atom. The convergence criteria for the geometry optimization were 2×10^{-5} eV/atom, 0.05 eV/Å and 0.002 Å for energy, force and displacement, respectively. To gain robust insight into the structure and electronic properties of perfect $BaCO_3$ and O-defect $BaCO_3$, the convergence of both the k-point Brillouin zone sampling and cutoff energy of the plane wave expansions in reciprocal space was tested. The converged results were obtained using PBE/USP with 9 × 6 × 9 −centred meshes (a total of 243 irreducible k-points) and a cutoff energy of 520 eV. Therefore, the results are discussed based on the 9 × 6 × 9 Monkhorst-Pack (MP) k-point sampling with 520 eV selected as the plane wave basis set cutoff energy.

The slab model of the O-defect $BaCO_3$ (130) facet was built by cleaving the bulk $BaCO_3$ crystal with the O-vacancy at the *c* site and consisted of an 9-layer-thick slab with three complete $BaCO_3$

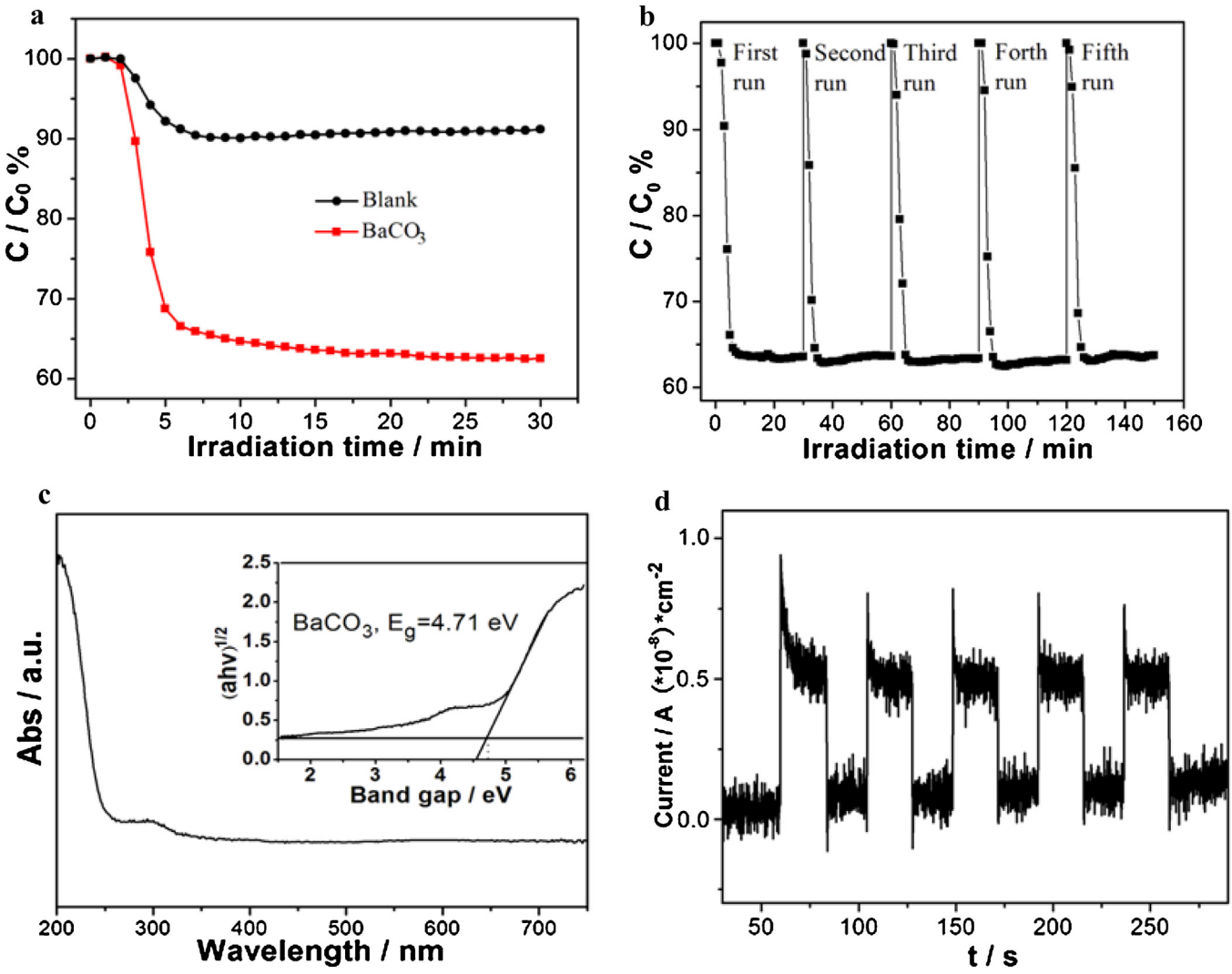

Fig. 3. (a) Photocatalytic activity of NO removal (λ = 280 nm). (b) Recycled testing. (c) UV–vis diffuse reflectance spectra of $BaCO_3$. (d) Transient photocurrent response of $BaCO_3$ under irradiation.

layers. A 10 Å thick vacuum layer was used to avoid the interaction between the repeated slabs. A $3 \times 1 \times 1$ *k*-space grid was used for structural relaxation to obtain the bare surface and absorption surface. The absorption energies of NO and O_2 molecules on the O-vacancy site were calculated according to

Eads = E(slab + adsorbate) − E(slab) − E(adsorbate), where E(slab + adsorbate), E(slab), and E(adsorbate) are the calculated electronic energies of the species adsorbed on the surface, the bare surface and the gas-phase molecule, respectively.

3. Results and discussion

3.1. Morphology and structure

$BaCO_3$ was synthesized by reacting $Ba(NO_3)_2$ and Na_2CO_3 in distilled water via a facile precipitation method at room temperature. Phase analysis based on X-ray diffraction data (Fig. S1, Supporting information) reveals that the as-prepared $BaCO_3$ sample consists of orthorhombic $BaCO_3$ (JCPDS#05-0378). Scanning electron microscopy (SEM, Fig. 1a) and transmission electron microscopy (TEM, Fig. S2, Supporting information) images demonstrate the particle-shaped morphology of the $BaCO_3$ sample. High-resolution TEM (HRTEM) (Fig. 1b) indicates that the as-prepared $BaCO_3$ is highly crystalline. The observed lattice fringes with interplanar lattice spacings of 0.320 nm in the bulk and 0.259 nm on the surface correspond to (002) and (130) facets of the $BaCO_3$ crystal, respectively. The difference in the lattice fringes between the bulk and surface of $BaCO_3$ may be caused by the surface orientation to reduce the surface energy. The surface area of the as-prepared $BaCO_3$ is determined to be 2.1 m^2/g (Fig. S3, Supporting information).

EDX point scans of the bulk and surface of the $BaCO_3$ sample indicate that the elemental distributions at the surface and in the bulk are similar (Fig. 2), implying the uniformity of the as-prepared $BaCO_3$ sample. The XPS survey spectrum also confirms the existence of Ba, C and O elements in the as-prepared $BaCO_3$ sample (Fig. S4, Supporting information). The high-resolution spectrum of Ba 3d with peak features at 795.2 eV (Ba $3d_{3/2}$) and 779.8 eV (Ba $3d_{5/2}$) suggests the presence of Ba^{2+}. The high-resolution O 1 s peak at 531.2 eV is associated with the C—O bond in CO_3^{2-} species. The C 1 s bands at 289.2 eV and 284.8 eV are ascribed to the existence of CO_3^{2-} and adventitious carbon species from the XPS measurement, respectively [19].

3.2. Photocatalytic activity, photoabsorption and photocurrent response

We initially investigated the photocatalytic removal of NO without the use of a photocatalyst as well as the photocatalytic effects

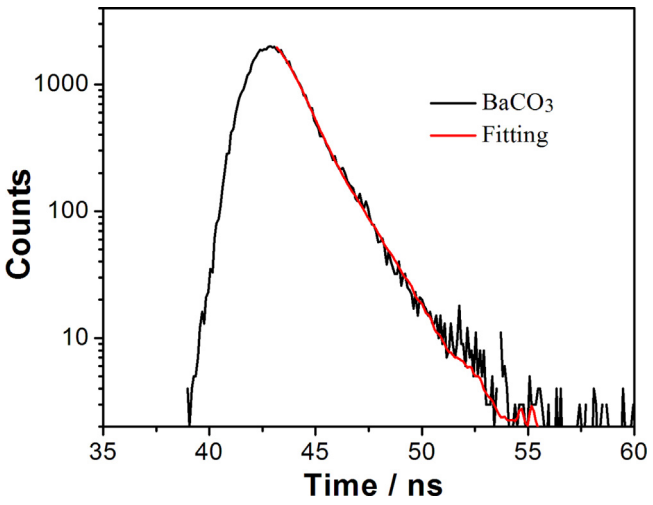

Fig. 4. Nanosecond-level time-resolved fluorescence spectra under 280 nm excitation at room temperature for $BaCO_3$.

of $BaCO_3$ for the removal of NO at room temperature. As shown in Fig. 3a, NO can be slightly removed under irradiation with a removal ratio of 10.0% in 30 min. However, upon using $BaCO_3$ as a photocatalyst, the removal ratio increases significantly to approximately 37.0%, suggesting that $BaCO_3$ exerts an unexpected photocatalytic activity for NO removal. An investigation of the photocatalytic durability demonstrates that the initial photocatalytic activity of $BaCO_3$ is almost completely maintained, even after five cycles (Fig. 3b). In addition, the as-prepared $BaCO_3$ is also effective for methyl orange (MO) degradation (Fig. S5). After irradiation for 360 min without photocatalysts, only 7.0% of MO is degraded, while the degradation ratio increases to 48.0% with the use of $BaCO_3$ as a photocatalyst (Fig. S5). Meanwhile, the colour of the MO solution becomes lighter. No other absorption peaks appear, indicating that MO is degraded instead of being transformed into other toxic materials (Fig. S6, Supporting Information). These results indicate that $BaCO_3$ exhibits an unprecedented photocatalytic activity for the removal of NO and degradation of MO, a phenomenon that has been conventionally regarded as impossible for insulator materials.

The optical properties of $BaCO_3$ were then probed using the ultraviolet-visible diffuse reflectance spectra, as shown in Fig. 3c. The absorption edge of $BaCO_3$ is located at approximately 250 nm, allowing the determination of the energy bandgap, 4.71 eV (Fig. 3c, inset). The experimental value of the bandgap is in good agreement with the reported value [15], implying that $BaCO_3$ is a typical insulator. However, it should be noted that an absorption peak at approximately 280 nm, corresponding to a bandgap of 4.43 eV, is observed in Fig. 3c, indicating that there are special optical absorption characteristics of the as-prepared $BaCO_3$.

Photoelectrochemical measurements were also performed, and the obtained results illustrated in Fig. 3d indicate that $BaCO_3$ exhibits certain photocurrent responses under UV light irradiation, meaning that electron (e^-)/hole (h^+) pairs can be produced upon photoexcitation. The photophysical properties of the photoexcited charge carriers of $BaCO_3$ were also analysed using nanosecond-level time-resolved fluorescence decay spectroscopy (Fig. 4). The fitting of the decay spectra gives two radiative lifetimes, $\tau_1 = 0.2051$ ns, $\tau_2 = 1.3339$ ns, for the as-prepared $BaCO_3$ samples, further confirming the generation of charge carriers under UV light irradiation.

3.3. Defects and DFT calculations of the electronic structure

There then arises the problem of how to elucidate the unexpected photocatalytic activity of $BaCO_3$. We believe that the unexpected photocatalytic activity is associated with the existence of some defects in the $BaCO_3$ crystal. It is well-known that crystal defect engineering is an effective method to extend the light response range of photocatalysts [20,21]. Since the reaction is conducted at room temperature and the reaction time is limited, defects can easily be introduced into the samples. To confirm this, *in situ* electron paramagnetic resonance (EPR) spectroscopy, a sensitive and direct method for probing crystal defects, was performed at 77 K to investigate the existence and nature of the defects in $BaCO_3$. As revealed by the results (Fig. 5a), under dark conditions, an EPR signal at $g = 2.024$ was observed that should be attributed to paramagnetic oxygen vacancies [22,23]. The peaks at $g_1 = 2.0012$, $g_2 = 2.0035$ and $g_3 = 1.9989$ can be ascribed to the presence of $^{\bullet}CO_2^-$ radicals formed by the removal of an oxygen atom from the CO_3^{2-} group [24,25]. Under light irradiation conditions, these signals are correspondingly intensified, further confirming that the prepared sample is sensitive to light. As electrons are excited and escape, more defects will be created. As expected, the experimental evidence confirms the existence of O-vacancy defects in $BaCO_3$.

Next, we explored how oxygen defects affect the electronic structure and subsequent photoexitation of $BaCO_3$. Density functional theory (DFT) calculations were performed to investigate the electronic structure of the perfect $BaCO_3$ and O-vacancy defect $BaCO_3$. First, the preference of the O-vacancy site in $BaCO_3$ was studied. The total energies of O-defect $BaCO_3$ indicate that the structure with an O-vacancy at site *c* is the most stable (Fig. 5b, the energy difference between this structure and the other structure is approximately 2.8 kJ/mol). The total density of states (TDOS) and partial density of states (PDOS) of the perfect $BaCO_3$ and the most stable O-defect $BaCO_3$ structures were calculated and are shown in Figs. 5c and 5d. Given density functional theory usually underestimates band gaps because of the discontinuity in the exchange-correlation potential, the calculated band gap of perfect $BaCO_3$ (4.46 eV), is in agreement with the experimentally predicted value (4.71 eV), which also indicates that $BaCO_3$ is a typical insulator. When an O-vacancy is present in $BaCO_3$, a middle level above the valence band (VB) appears in the band gap structure of $BaCO_3$, endowing $BaCO_3$ with extended light absorption.

PDOS analysis reveals that O-vacancy defects in $BaCO_3$ induce a significant shift of the energy band toward the low-energy region (Fig. 6) and also that some new levels appear in the neighbourhood of the Fermi level in O-vacancy defect $BaCO_3$. Based on the atom-resolved PDOS (Fig. 7), these new levels can be ascribed to the presence of $^{\bullet}CO_2^-$ species that are formed via the removal of oxygen atoms from CO_3^{2-}. The middle level can be ascribed to the contribution of the *p* states of the C and O atoms in $^{\bullet}CO_2^-$, similar to that of the valence band maximum. This implies that $^{\bullet}CO_2^-$ species play a vital role in the band structure construction and facilitate electron excitation under irradiation. In other words, photoexcited electrons can easily jump from the middle level to the conduction band under irradiation. These transition processes could yield charge carriers.

3.4. Active species, DFT calculations of the adsorption energy and in situ *DRIFTS spectra*

To explore the photocatalytic mechanism, holes and electrons-trapping experiments were performed using potassium iodide and potassium dichromate as the scavengers, respectively (Fig. S7, Supplementary information) [26]. Addition of both potassium dichromate or potassium iodide reduces the removal of NO, indicating that holes and electrons play important roles in the photocatalytic oxidation of NO. Moreover, the DMPO spin-trapping ESR spectra in an aqueous dispersion for DMPO-$^{\bullet}OH$ and in a methanol dispersion for DMPO-$^{\bullet}O_2^-$, respectively, were measured. As seen from Fig. 8a, signals of the hydroxyl radical ($^{\bullet}OH$) cannot

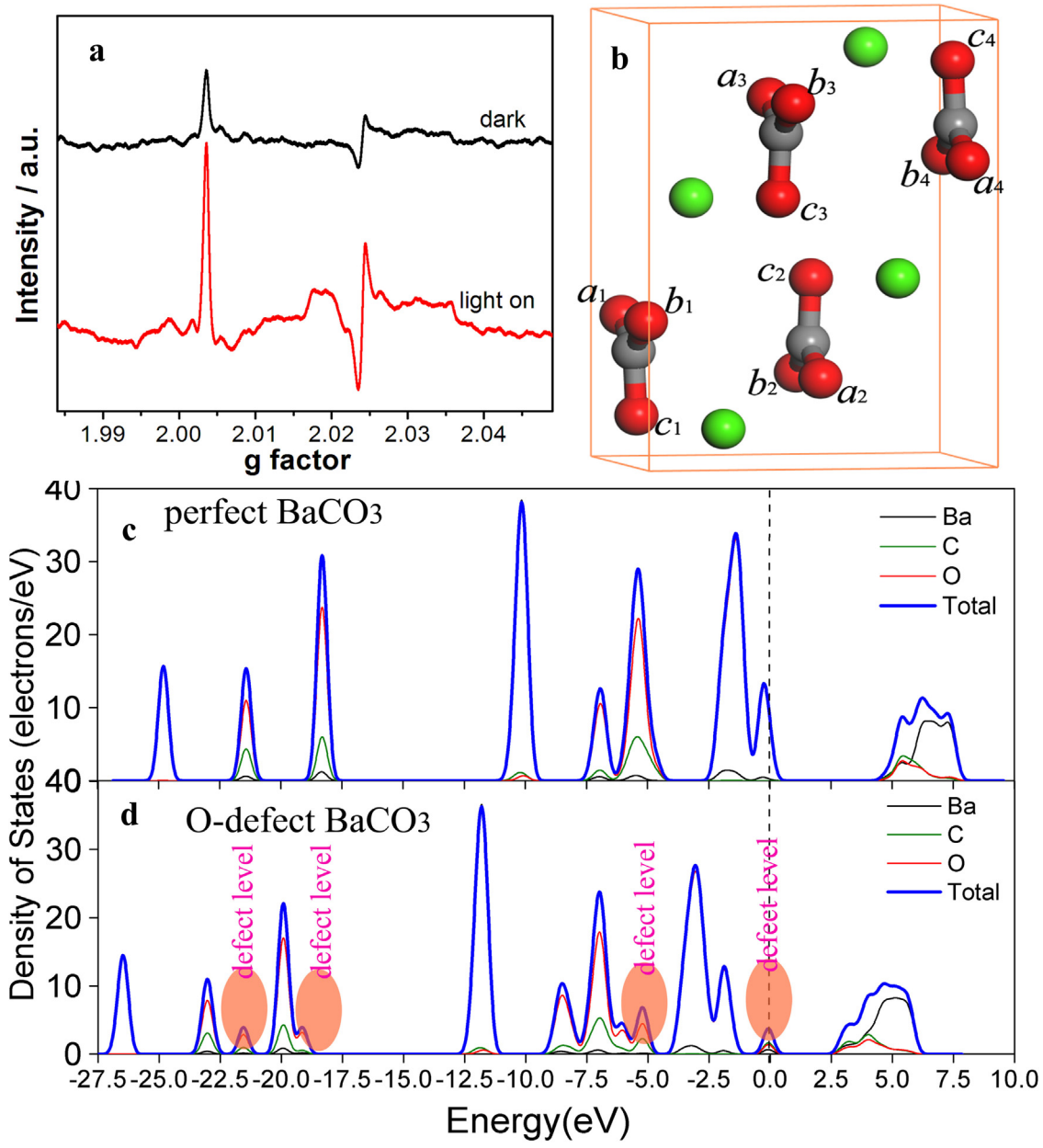

Fig. 5. (a) EPR spectra of the as-prepared $BaCO_3$ at 77 K. (b) Schematic presentation of O atom sites in $BaCO_3$. (c) Calculated DOS of perfect $BaCO_3$. (d) Calculated DOS of O-defect $BaCO_3$.

be observed, but those of the superoxide anion radical ($^{\bullet}O_2^-$) were present. This means that in the photocatalytic reaction, $^{\bullet}O_2^-$ rather than ·OH plays an important role in NO removal.

The adsorption of NO and O_2 molecules on the O-vacancy site was investigated based on the slab model of O-defect $BaCO_3$ with the (130) facet. The optimized geometries of adsorption complexes are depicted in Figs. 8b and 8c. The adsorption energies of NO and O_2 are calculated to be 24.3 and 63.7 kcal/mol, respectively, indicating that both NO and O_2 can be stably adsorbed at the O-vacancy site, with the O_2 adsorption on the O-vacancy site more thermodynamically favourable than NO adsorption. For the case of adsorbed O_2, the O—O bond length was elongated to 1.50 Å from 1.24 Å in the isolated O_2 molecule. For the adsorbed NO, the N—O bond length is elongated to be 1.40 Å from 1.19 Å in the isolated NO molecule. These results imply that O—O and N—O bonds are weakened and thus that O_2 and NO molecules are activated by adsorption on the O-vacancy site.

Then, *in situ* DRIFTS studies were performed to further understand the photocatalytic removal of NO. In the dark, introducing $NO + O_2$ to the $BaCO_3$ sample results in the appearance of various bands, as shown in Fig. 8d. The band at 1254 cm^{-1} is attributed to bidentate nitrate [27]. Additionally, bands at 1317 cm^{-1}, 1340 cm^{-1} and 1363 cm^{-1}, which are associated with nitrol species, can be observed.[22] Under light irradiation, the bands related to the nitrol species strengthen and the band at 1254 cm^{-1} becomes negative, meaning that bidentate nitrate is transformed to other species. Additionally, several new bands appear. Nitrates with bands at 1066, 1222, 1232 and 1280 cm^{-1} and NO^- with bands at approximately 1145 and 1172 cm^{-1} are developed [28,29]. In addition, bands associated with nitrite are detected at 1202, 1108 and 1353 cm^{-1} [30–32]. These bands are strengthened with the increased irradiation time. Thus, we conclude that NO is adsorbed in the form of bidentate nitrate and nitrosyls species that can then easily react with e^-, h^+ and $\cdot O_2^-$ generated under irradiation to

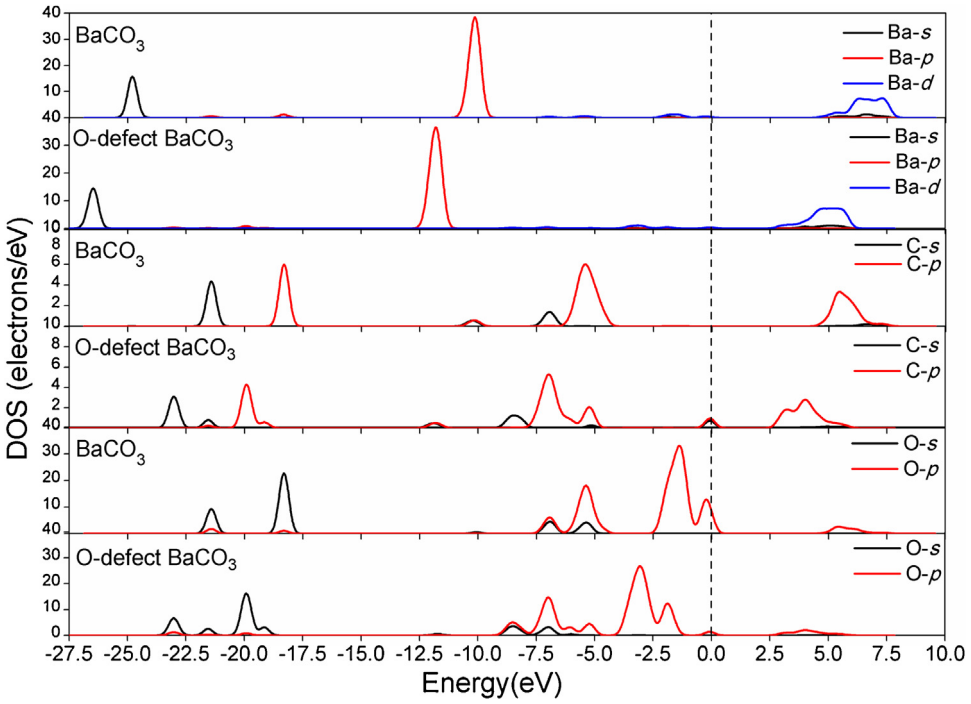

Fig. 6. The partial density of states (PDOS) of perfect $BaCO_3$ and O-defect $BaCO_3$.

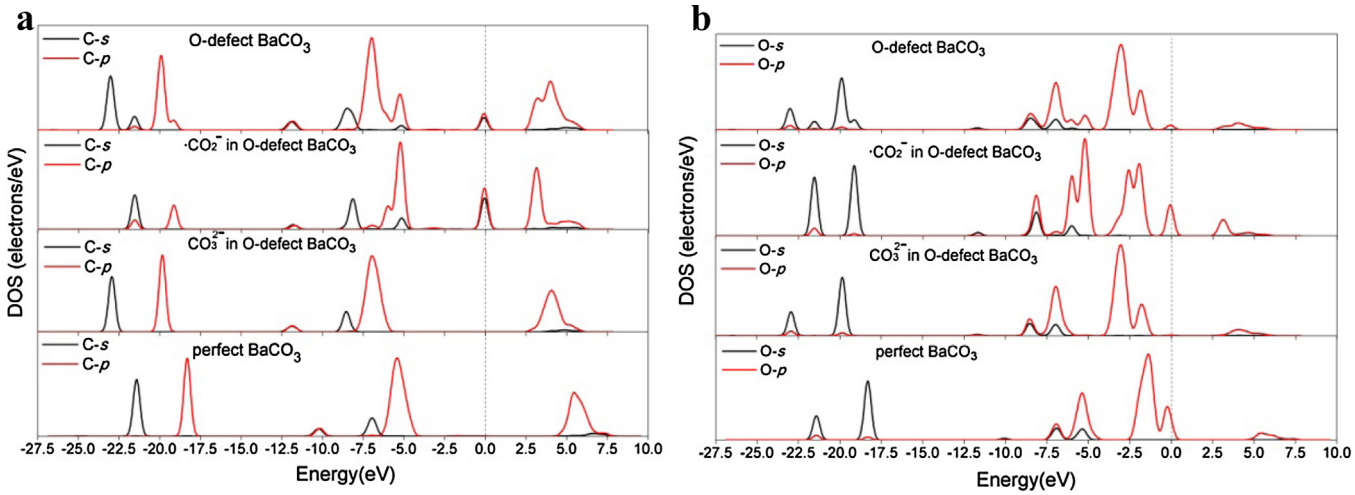

Fig. 7. (a) The density of states of carbon atom in CO_3^{2-} and $\cdot CO_2^-$ groups in O-defect $BaCO_3$. (b) The density of states of oxygen atom in CO_3^{2-} and $\cdot CO_2^-$ species in O-defect $BaCO_3$. As can be seen from them, the new levels arise near Fermi level can be ascribed to the contribution of $\cdot CO_2^-$ species, implying the important role of O-defect in O-defect $BaCO_3$.

transform into free nitrites and nitrates ions. The inorganic NO_3^- ions accumulated on the surface of the photocatalyst can be easily removed by water washing.

3.5. Photocatalysis mechanism

Based on the experimental and theoretical studies described above, we propose a photocatalysis mechanism of $BaCO_3$ for NO removal, as depicted in Fig. 9. First, under 280 nm irradiation, $BaCO_3$ with O-vacancy defects are photoexcited to produce photoinduced electrons and holes (Eq. (1)), and then, the excited electrons react with O_2 to yield $^{\bullet}O_2^-$ to initiate chemical reactions (Eq. (2)-(3)) or directly with NO to create NO^- (Eq. (4)). On the other hand, the photogenerated holes directly oxidize NO. The *in situ* FT-IR spectra and adsorption calculations suggest a photocatalytic mechanism for NO removal involving the adsorbed species in the dark and active species generated under 280 nm irradiation (Eq. (1)–(7)).

$$BaCO_3 + UVlight(280\,nm) \rightarrow h^+(BaCO_3) + e^-(BaCO_3) \quad (1)$$

$$e^- + O_2 \rightarrow {}^{\bullet}O_2^- \quad (2)$$

$$^{\bullet}O_2^- + NO \rightarrow NO_3^- \quad (3)$$

$$e^- + NO \rightarrow NO^- \quad (4)$$

$$NO^- + O_2 \rightarrow NO_3^- \quad (5)$$

$$H_2O + h^+ + NO \rightarrow NO_2^- + 2H^+ \quad (6)$$

$$2H_2O + 3\,h^+ + NO \rightarrow NO_3^- + 4H^+ \quad (7)$$

Inspired by this surprising finding, we prepared other insulators, such as sulphate and phosphate compounds, according to room

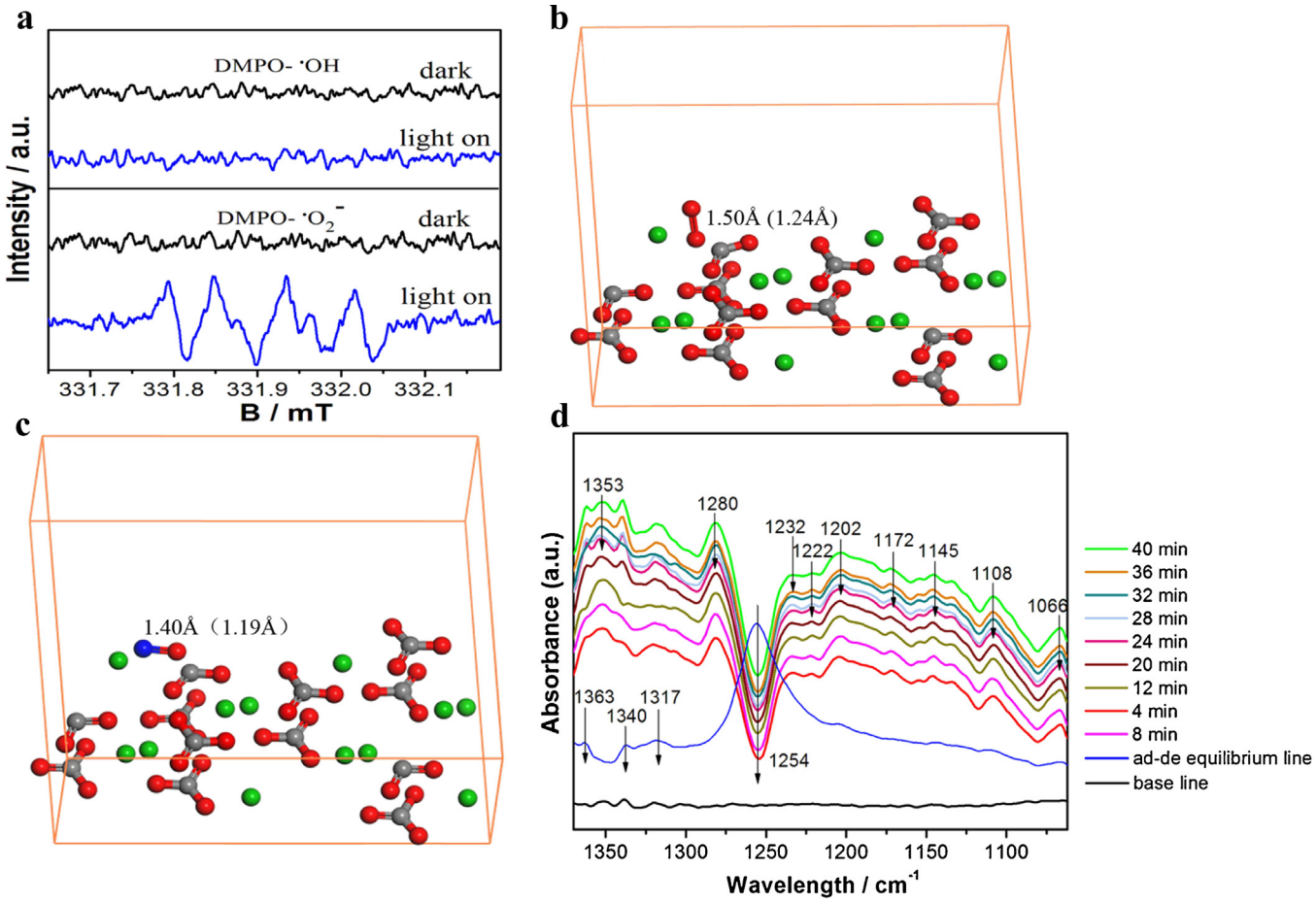

Fig. 8. (a) DMPO spin-trapping ESR spectra of $BaCO_3$ in an aqueous dispersion for DMPO-·OH and in a methanol dispersion for DMPO-·O_2^- under 280 nm light irradiation. (b, c) Optimized geometries of adsorption complexes. (d) *In situ* DRIFTS spectra of $BaCO_3$ treated in flowing 50 ppm NO (50 mL/min) at room temperature in the dark for 60 min to reach adsorption-desorption equilibrium and then under irradiation for 40 min.

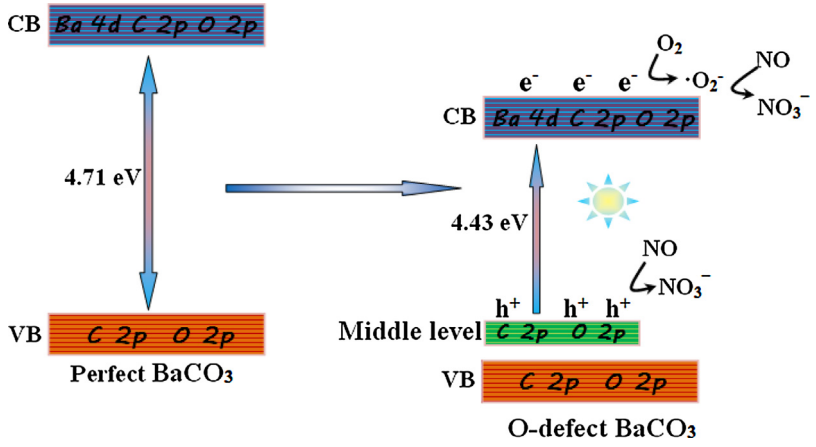

Fig. 9. Photocatalysis mechanism of $BaCO_3$ under 280 nm light irradiation.

temperature precipitation methods (Fig. S8a, Supplementary information). It is exciting to find that all of these materials show a certain photocatalytic performance toward the removal of NO as well (Fig. S8b, Supplementary information). This work describes a new family of photocatalysts and expands the range of photocatalysts to insulator materials. Also, as the O-vacancy plays key a role in photocatalysis, we will try to tune the content of O-vacancy in the insulators by H_2 treatment or other chemical reduction method to optimize the photocatalysis efficiency in the future work. As is well-known, sulphates, carbonates and phosphates are earth-abundant in the nature, so this research indicates that photocatalysis occurs when these types of salts in the earth are exposed to solar light irradiation and thus provides new insights into the nitrogen cycle.

4. Conclusion

In summary, we demonstrated for the first time that $BaCO_3$ could be used as a promising photocatalyst for NO removal, with

an approximately five-fold enhancement observed for the removal of NO with the use of $BaCO_3$ as a photocatalyst. The experimental and theoretical calculation results reveal that the O-vacancy defects should be responsible for the unexpected photocatalytic activity of the as-prepared $BaCO_3$. The O-vacancy defects in $BaCO_3$ give rise to a new level in the gap between the valence and conduction bands. This unique electronic structure significantly facilitates the separation of electron-hole pairs to produce photogenerated electrons and hole, and then induces the production of several active radical species, such as $^{\bullet}O_2^-$, that play key roles in the NO removal reaction. Interestingly, other insulators, such as sulphate and phosphate compounds, are also found to display photocatalytic performance. The discovery of $BaCO_3$ and other sulphates and phosphates as insulator photocatalysts is of great significance as it is expected to shed new light on the understanding and application of earth-abundant insulator photocatalysts. The present work opens a new important area in materials science and provides new insights into the nitrogen cycle on earth. We believe that the present study will also open up a new important area for the development of photocatalysts owing to the promising catalytic activities, low cost, environmental friendliness and natural abundance of the studied materials.

Acknowledgment

This work was supported by the National Key R&D project (2016YFC0204702), the National Natural Science Foundation of China (51478070, 21501016 and 51108487), the Innovative Research Team of Chongqing (CXTDG201602014) and the Key Natural Science Foundation of Chongqing (cstc2017jcyjBX0052).

Appendix A. Supplementary data

Supplementary data associated with this article can be found, in the online version, at http://dx.doi.org/10.1016/j.apcatb.2017.07.082.

References

[1] M.R. Hoffmann, S.T. Martin, W. Choi, D.W. Bahnemann, Chem. Rev. 95 (1995) 69–96.
[2] Y. Ma, X. Wang, Y. Jia, X. Chen, H. Han, C. Li, Chem. Rev. 114 (2014) 9987–10043.
[3] J. Liu, Y. Liu, N. Liu, Y. Han, X. Zhang, H. Huang, Y. Lifshitz, S.T. Lee, J. Zhong, Z. Kang, Science 347 (2015) 970–974.
[4] S. Ghosh, N.A. Kouamé, L. Ramos, S. Remita, A. Dazzi, A. Deniset-Besseau, P. Beaunier, F. Goubard, P.H. Aubert, H. Remita, Nature Mater. 14 (2015) 505–511.
[5] W. Dong, D. Wu, J. Luo, Q. Xing, H. Liu, J. Zou, X. Luo, X. Min, H. Liu, S. Luo, C. Au, J. Catal. 349 (2017) 218–225.
[6] J. Zou, J. Ma, Q. Huang, S. Luo, J. Yu, X. Luo, W. Dai, J. Sun, G. Guo, C. Au, S.L. Suib, Appl. Catal. B 156-157 (2014) 447–455.
[7] X. Wang, K. Maeda, A. Thomas, K. Takanabe, G. Xin, J.M. Carlsson, K. Domen, M. Antonietti, Nature Mater. 8 (2009) 76–80.
[8] Z. Yi, J. Ye, N. Kikugawa, T. Kako, S. Ouyang, H. Stuart-Williams, H. Yang, J. Cao, W. Luo, Z. Li, Y. Liu, R.L. Withers, Nature Mater. 9 (2010) 559–564.
[9] L. Liao, Q. Zhang, Z. Su, Z. Zhao, Y. Wang, Y. Li, X. Lu, D. Wei, G. Feng, Q. Yu, X. Cai, J. Zhao, Z. Ren, H. Fang, F. Robles-Hernandez, S. Baldelli, J. Bao, Nat. Nanotech. 9 (2014) 69–73.
[10] R. Asahi, T. Morikawa, H. Irie, T. Ohwaki, Chem. Rev. 114 (2014) 9824–9852.
[11] J. Zou, L. Wang, J. Luo, Y. Nie, Q. Xing, X. Luo, H. Dua, S. Luo, S.L. Suib, Appl. Catal. B 193 (2016) 103–109.
[12] F. Dong, T. Xiong, Y. Sun, Z. Zhao, Y. Zhou, X. Feng, Z. Wu, Chem. Commun. 50 (2014) 10386–10389.
[13] L. Zhou, C. Zhang, M.J. McClain, A. Manjavacas, C.M. Krauter, S. Tian, F. Berg, H.O. Everitt, E.A. Carter, P. Nordlander, N.J. Halas, Nano Lett. 16 (2016) 1478–1484.
[14] R. Li, X. Wang, S. Jin, X. Zhou, Z. Feng, Z. Li, J. Shi, Q. Zhang, C. Li, Sci. Rep. 5 (2015) 13475.
[15] J.E. Saal, S. Kirklin, M. Aykol, B. Meredig, C. Wolverton, JOM 65 (2013) 1501–1509.
[16] S. Lv, P. Li, J. Sheng, W. Sun, Mater. Lett. 61 (2007) 4250–4254.
[17] S.J. Clark, M.D. Segall, C.J. Pickard, P.J. Hasnip, M.I.J. Probert, K. Refson, M.C.Z. Payne, Kristallogr 220 (2005) 567–570.
[18] J.P. Perdew, K. Burke, M. Ernzerhof, Phys. Rev. Lett. 77 (1996) 3865–3868.
[19] P.J. Schmitz, Surf. Sci. Spectra 8 (2001) 190–194.
[20] X. Chen, L. Liu, P.Y. Yu, S.S. Mao, Science 331 (2011) 746–750.
[21] L. Liu, X. Chen, Chem. Rev. 114 (2014) 9890–9918.
[22] C. Drouilly, J.M. Krafft, F. Averseng, S. Casale, D. Bazer-Bachi, C. Chizallet, V. Lecocq, H. Vezin, H. Lauron-Pernot, G. Costentin, J. Phys. Chem. C 116 (2012) 21297–21307.
[23] Y. Su, J. Lang, L. Li, K. Guan, C. Du, L. Peng, D. Han, X. Wang, J. Am. Chem. Soc. 135 (2013) 11433–11436.
[24] V. Natarajan, T.K. Seshagiri, A.G.J. Page, Radioanal. Nucl. Chem. 187 (1994) 123–129.
[25] F. Köksal, D. Demir, R. Köseoğlu, M. Birey, A. Köroğlu, Appl. Magn. Reson. 29 (2005) 205–210.
[26] J. Wang, Y. Yu, L. Zhang, Appl. Catal. B: Environ. 136–137 (2013) 112–121.
[27] J.C.S. Wu, Y.T. Cheng, J. Catal. 237 (2006) 393–404.
[28] K. Hadjiivanov, H. Knözingerb, Phys. Chem. Chem. Phys. 2 (2000) 2803–2806.
[29] K. Hadjiivanov, V. Avreyska, D. Klissurski, T. Marinova, Langmuir 18 (2002) 1619–1625.
[30] M. Kantcheva, A.S. Vakkasoglu, J. Catal. 223 (2004) 352–363.
[31] H. Miyata, S. Konishi, T. Ohno, F. J. Chem. Soc. Hatayama, Faraday Trans. 91 (1995) 1557–1562.
[32] Q. Sun, Z.X. Gao, H.Y. Chen, W.M.H. Sachtler, J. Catal. 201 (2001) 89–99.